PROCESS - PROPERTY CORRELATION OF FRICTION STIR WELDING OF MARINE GRADE ALUMINIUM ALLOY 5083 USING FINITE ELEMENT ANALYSIS

(Reference No: IJME632a, DOI No: 110.5750/ijme.v163iA2.757)

M Sahu, National Institute of Technology Raipur, India, **A Paul**, Indian Institute of Technology Kharagpur, India, and **S Ganguly**, National Institute of Technology Raipur, India

KEY DATES: Submitted: 18/12/20; Final acceptance: 05/01/21; Published 12/07/21

SUMMARY

In this article, a 3D finite element based thermo-mechanical model for friction stir welding (FSW) of a marine-grade aluminium alloy 5083 is proposed. The model demonstrates the thermal evaluation and the distribution of residual stresses and strains under the variation of process variables. The temperature profile of the weld joint during the FSW process and the mechanical properties of the joints are also experimentally evaluated. The necessary calibration of the model for the correct implementation of the thermal loading, mechanical loading, and boundary conditions was performed using the experimental results. The model simulation and experimental results are analyses in view of the process-property correlation study. The residual stress was evaluated along, and across the weld, centreline referred as longitudinal and transverse residual stresses, respectively. The magnitude of longitudinal residual stress is noted 60-80% higher than that of the transverse direction. The longitudinal residual stress generated a tensile oval shaped stress region around the tool shoulder confined to a maximum distance of about 25mm from the axis of the tool along the weld line. It encompasses the weld-nugget to thermo-mechanically affected zone (TMAZ), while the parent metal region is mostly experiences the compressive residual stresses. However, the transverse residual stress region appears like wing shaped region spread out in both the advancing and retreating side of the weld and occupying approximately double the area as compared to the longitudinal residual stresses. Overall, the study revealed a corelation between the FSW process variables such as welding speed and the tool rotational speed with the residual stress and the mechanical properties of the joint.

NOMENCLATURE

C_P	*Specific Heat (J Kg^{-1} m^{-3})*
E	*Elastic Youngs Modulus (G Pa)*
K	*Thermal heat Transfer Coefficient (W m^{-1}°C^{-1})*
UTS	*Ultimate Tensile Strength (M Pa)*
α	*Coefficient of Thermal Expansion (10^{-6} °C^{-1})*
Δ	*Percentage Deviation in Experimental and Simulated Peak Temperature (%)*
μ	*Poisson's Ratio*
v	*Welding Speed Rate (mm min^{-1})*
ρ	*Mass Density (g cm^{-3})*
τ	*Time (s)*
RPM	*Tool Rotational Speed*
T_E^{max}	*Peak Temperature obtained from Experiment (°C)*
T_S^{max}	*Peak Temperature obtained from Simulation (°C)*

1. INTRODUCTION

Friction Stir Welding (FSW) technique is devised by Wayne Thomas at The Welding Institute (TWI) Ltd, Cambridge, in the year 1991(Thomas *et al.*, 1991). From that date only, the technique is effectively utilised in automotive, shipbuilding, railways, defence, aerospace industries for joining low melting temperature materials like aluminium, brass, copper, and also high melting temperature materials like steels (Kouadri-Henni and Barrallier, 2014), nickel (Ayer *et al.*, 2005) and titanium-based alloys (Reynolds, Hood and Tang, 2005). The process does not involve any utilisation of consumables, filler wire, shielding gases (Jin *et al.*, 2001) and thus, eliminates the problems associated with the solidification of fused material (Çam and Mistikoglu, 2014).

FSW process utilises a non-consumable rotating tool which plasticises the material, and a horizontal welding speed is provided to the tool along the joint line, producing a defect-free & high quality of welds. The material undergoes severe plastic deformation at elevated temperature, producing ultrafine and equiaxed grains which result in welds of excellent mechanical properties (Jata, 2009). Proper selection of tool geometry and parameters plays a vibrant role in governing the quality of the weld joints (Mishra and Ma, 2005).

To maintain precision about mechanics and thermodynamics involved in the process and to minimise the experimental work, various computational frameworks have been adopted. Finite Element Method (FEM) is the most prominent & promising computational simulation techniques utilised by the researchers for the modelling of FSW, which provides a precise & deep understanding about the process. Various models have been proposed in the past literature elaborating the heat flow (Bjørneklett *et al.*, 1999) (Frigaard, Grong and

Midling, 2001) and material movement to understand the complex thermomechanical phenomena's involved in FSW (Dong *et al.*, 2013). Some researchers have proposed welding simulation code like "WELDSIM" (Zhu and Chao, 2002) and "DEFORM" (Uyyuru and Kailas, 2006), for studying the residual stress, strain rate and distortion occur during the welding process. A few reported works in the field of enhancing the thermal efficiency and stability of the welding process (Dickerson, Shi and Shercliff, 2003), the study of time-temperature history (Chen and Kovacevic, 2003), the mechanism behind the contact conditions between the rotating tool and workpiece (Schmidt, Hattel and Wert, 2004), has also been reported. Analytical models for process property correlation (Buffa *et al.*, 2006a), examining the material flow behaviour (Buffa *et al.*, 2006b) and evaluating the interfacial stress between the workpiece and backplate (Soundararajan, Zekovic and Kovacevic, 2005) are few other focused area in this field.

In last two decade, a bulk of analytical or numerical simulations have been carried out, and only a few of them (Zhu and Chao, 2004a)(Chen and Kovacevic, 2003)(Soundararajan, Zekovic and Kovacevic, 2005)(Buffa *et al.*, 2006a) emerged as the plausible tool for realistic simulation of the process. This is because of the difficulty in the complete mapping of actual and real-time welding onto the simulation platform. Therefore, developing an effective model for the FSW process in a much more realistic framework is contextually important. In the present work, a 3-D nonlinear thermo-mechanical model is developed, based on finite element method, which not only simulate a realistic physical environment of the actual process but also enable to analyse the process for better join performance. The simulation is carried out in ANSYS APDL software. The model is utilised to explore insight about the temperature contours, residual stresses and strains generated during FSW at different operational conditions. This article attempted to present an insight to study the process property correlation by exploiting the influence of various FSW parameters on the simulated time-temperature history, the residual stresses and the experimentally determined tensile stress.

2. MATERIALS AND METHODS

This section presents the detail description of the material, FSW process setup, experimental and computational details.

Table 1: Chemical composition of AA5083 in weight %

Mg	Mn	Cr	Si	Fe	Cu	Al	Others
4.67	0.70	0.12	0.04	0.02	0.08	95.99	Balance

2.1 MATERIAL

Two 150mm X 60mm X 5mm plates of AA5083 is used in the present investigation. The chemical composition of the as-received sheet is presented in Table 1. The hardness of the as-received sheets was recorded as 92 VHN.

2.2 FSW SETUP AND EXPERIMENTAL

The plates were placed in a butt configuration upon a horizontal milling machine (Balboa Machine Tools Limited make) with a vertical attachment specially prepared for FSW. The schematic of the welding setup is shown in Figure 1. The welding was carried out at two welding speeds of 56 mm per minute and 28 mm per minute, and two rotational speeds – 710 and 1000 rpm. The configuration of the tool utilised in the present study is straight cylindrical pin with shoulder diameter as 27.1 mm and pin diameter as 5.4 mm. The details of the experimental plan, along with the welding variants, are shown in Table 2. A K-type thermocouple was fitted in an arrangement, as shown in Figure 1, for recording the maximum temperature generated during welding. A constant plunge force of 5 KN was applied for all the FSW trials.

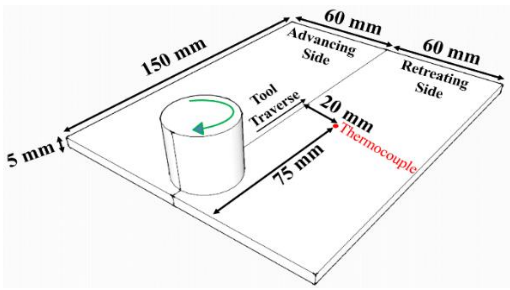

Figure 1: Schematic representation of the welding setup for FSW joining of AA5083.

The tensile testing was carried out at room temperature on an INSTRON 1342 Servo Hydraulic Material Testing Machine having static and dynamic loading capacity of 0 to 250 KN & a crosshead velocity of 2.5 mm/min is maintained. All the testing samples were cut with wire cut EDM with required dimensions as per ASTM E8 standards. The schematic picture of the tensile test sample is represented in Figure 2(a).

Table 2: Sample designation and experiment matrix for the fabrication of FSW joints

Sample Designation	Rotational Speed	*v*
S1	1000	28
S2	710	28
S3	1000	56
S4	710	56

The Vickers microhardness tests were performed with Vickers's Hardness Testing Machine (OLYMPUS U-PMTVC 4F06790, Japan). The hardness was taken with an interval of 1 mm across the weld centre line to the base metal zone in both the side applying a 10-g load with 10 seconds of dwell time. The microstructural evolution through electron backscattered diffraction (EBSD) study was performed in a Field emission scanning electron microscope (FE-SEM), make JSM-7100F while the samples were prepared using electropolishing technique with A2 electrolyte. The collection of sample materials from the weld joint for different tastings are schematically illustrated in Figure 2.

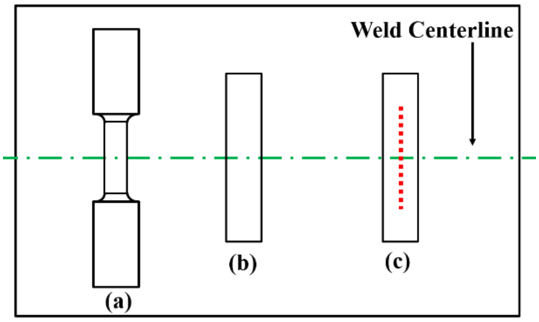

Figure 2: Schematic illustration of collection of sample materials from the FSW joint for (a) tensile, (b) microstructure evolution and (c) microhardness test specimen

2.3 COMPUTATIONAL DETAILS

In this study, a computational framework has been developed implementing the 3D finite element-based technique to model the thermo-mechanical evolution of the FSW process applied to marine grade AA5083. The formulation of the thermal profile is done following the Fourier law of 3D uniform heat conduction equation mentioned as (1).

$$\rho C_p \frac{\partial T}{\partial \tau} = \frac{\partial}{\partial x}\left(K_x \frac{\partial T}{\partial x}\right) + \frac{\partial}{\partial y}\left(K_y \frac{\partial T}{\partial y}\right) + \frac{\partial}{\partial z}\left(K_z \frac{\partial T}{\partial z}\right) \qquad (1)$$

In this context, the assumptions made while defining the input conditions and creating geometry for simulation are (i) the frictional coefficient is considered to be constant as 0.5 at the tool-workpiece interface (Frigaard, Grong and Midling, 2001); (ii) the geometry of tool pin has been taken as straight cylindrical; and (iii) the heat loss due to radiation has been neglected. The modelling is done in two parts (A) Workpiece, and tool modelling and the other is (B) Contact pair modelling. Both the parts are described separately below. The temperature reliant material properties (specific heat, thermal conductivity, and density) used in this work for workpiece and the tool materials has been shown in Table 3 and Table 4, respectively. The workpiece and tool are considered to have isotropic material properties.

Table 3: Temperature-dependent material properties for workpiece material AA5083 used in the thermo-mechanical model (Zhu and Chao, 2004b)

Temperature	***K***	***C_P***	***ρ***
20	112.5	942.1	2673.9
80	122.7	984.2	2642.7
180	131.6	1039.6	2629.4
280	142.3	1081.2	2611.5
380	152.5	1136.6	2589.3
480	159.5	1178.2	2567.0
580	177.2	1261.4	2549.2

Table 4: Material properties for tool material AISI 310 austenitic grade stainless steel used in the thermo-mechanical model

E	***μ***	***K***	***C_p***	***ρ***	***α***
520	0.22	20	600	7800	17

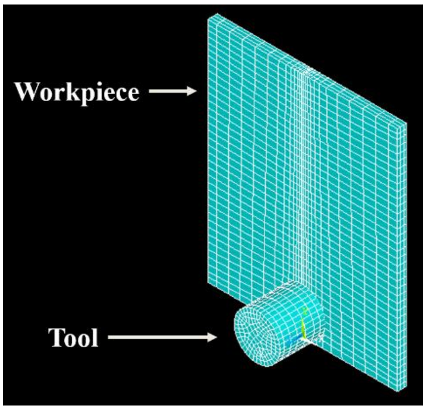

Figure 3: Workpiece and tool model used in the thermo-mechanical simulation

2.3 (a) Workpiece & Tool Setup for Simulation

Both the plates and the tool are modelled with a coupled-field element, SOLID226, keeping the dimensions the same as that used during experimental trials. Fine hexahedral mesh has been used (Chao, Qi and Tang, 2003). The pictorial arrangement of the FSW setup for FE simulation has been shown in Figure 3.

2.3 (b) Contact Pair Modeling

Two contact pairs are introduced in the model. First contact pair is established between the interface of the plates to be welded. It is a usual surface-to-surface contact pair established using the TARGE170 and CONTA174 elements, as shown in Figure 4.

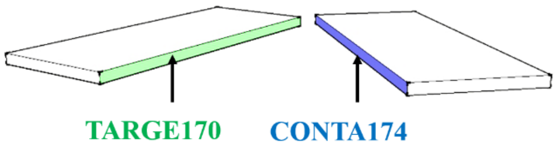

Figure 4: Schematic illustration of the contact pair maintained between the plates in the thermo-mechanical simulation

This contact pair is assigned with a large thermal contact conductance (TCC) value of 2e6 W/m^2 °C (Kumar Thimmaraju, Arkanti and Chandra Mohan Reddy, 2018) along with a bonding temperature of 300 ^{o}C (Mohan *et al.*, 2014) to simulate continuous bonding between them.

The second contact pair is established between the top surface of the plates and the tool. It is a normal surface-to-surface contact pair which has been established with CONTA174 element to mesh TARGE170 element have meshed the top surface of the workpiece and the corresponding tool surfaces in contact with the top surface. This formulation has been described in, as shown in Figure 5.

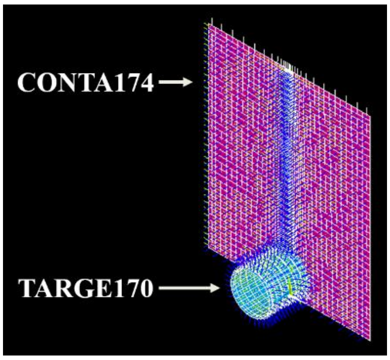

Figure 5: Schematic illustration of the contact pair established between tool and workpiece in the thermo-mechanical model

This contact pair is specified with three real constants. The first real constant is the FHTG, which is assigned a value of 1. The next real constant is FWGT which is assigned with a fractional value of 0.95 (Chao, Qi and Tang, 2003). The contact pair is assigned with a low thermal contact conductance (TCC) value of 10 W/m^2 °C. Moreover, a pilot node of TARGE170 element is rigidly bonded with the nodes of the top surface of the tool, which is made of CONTA174 element.

2.3 (c) Boundary Conditions

The model is assigned to both thermal and mechanical boundary conditions. Under thermal boundary condition, for all external surfaces of the plates other than the bottom surface, the convective heat transfer coefficient is 30 W/m^2 °C, and that of for the bottom surface of the workpiece is 350 W/m^2 °C following the work in reference (Prasanna, Rao and Rao, 2010). The uniform temperature of 25°C is assigned as the initial temperature boundary condition to the entire model. Under mechanical boundary conditions, the workpiece is kept fixed in all the load steps of simulation. The transient analysis is done with large deformation effect in addition to ramped loading. The entire simulation is split into three load steps, each of which is a replica of the three steps during the experimental FSW process as plunge, dwell, and traverse. The maximum time step is restricted to 0.03 to reduce the simulation time.

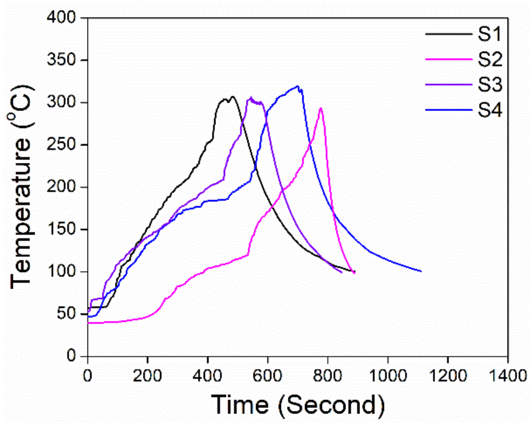

Figure 6: Time-temperature history of the fabricated friction stir welded sample from experimental trials.

3. RESULTS AND DISCUSSION

3.1 THERMAL PROFILE OF THE FSW PROCESS

Figure 6 represents the time vs temperature curve obtained from the experimental welding trials. The peak temperature raised during welding is one of the most important factors. It governs the evolution of finer microstructure through recrystallisation and grain refinement and thus, eventually the quality of the welds. It can be seen from the temperature contours that the peak temperature in all the specimen (S1 to S4) is lower than the melting temperature of the alloy, i.e., ~630 ^{o}C. This result anticipates that the FSW joining is a solid-state process. On the other hand, Figure 7 shows the simulated temperature profile of the FSW joints obtained from the proposed model. It is worthy to note that the simulation results hold a decent agreement with the trend observed in experimentally measured temperature profiles (see Figure 6 and 7).

The close match of the pattern of the thermal profile and the recorded peak welding temperature under the different FSW operation conditions, i.e., change in rotational speed and welding speed depicted the proper calibration of the model and qualifying the model for further analysis and use. The influence of FSW parameters on the evolution of thermal profile and mechanical properties has been discussed in the following subsections.

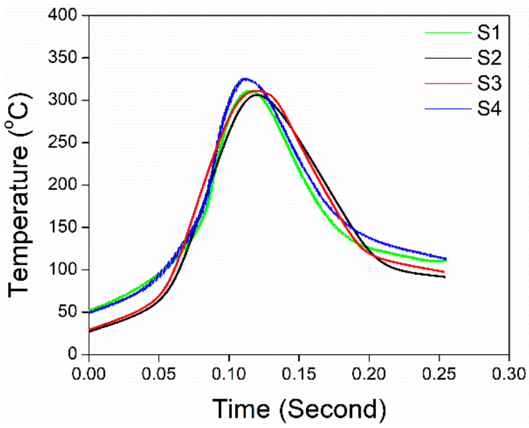

Figure 7: Simulated time-temperature history of welded samples obtained from the thermo-mechanical model.

3.1(a) Influence of Rotational Speed (RPM) on time-temperature History

Table 5 presents the detailed comparison of experimental and simulated temperature profiles showing the influence of rotational speed in the evolution of temperature profile. The deviation in the profiles is accounted for in an appreciable range of less than 4% (in Table 5). Such a small deviation indicates that the simulation model closely represents the real experimental situation of FSW. Thus, the model has been validated and qualify for the subsequent analysis of process -property correlation study. The analysis of the experimental results recorded the peak temperature of sample S1 as 308.25 °C and the peak temperature of sample S2 as 293.691 °C while welding speed remains constant at 28 mm per minute.

Table 5: Effect of tool rotational speed on peak temperature, on keeping the welding speed rate constant

Sample	**RPM**	***v***	T_E^{max}	T_S^{max}	**Δ**
S1	1000	28	308.205	317.67	3.07
S2	710	28	293.721	304.508	3.67

The increase in peak temperature in the case of sample S1 (1000 rpm rotational speed) as against the sample S2 (710 rpm rotational speed) can be attributed as because of the high frictional heat generation. Large power input through the mechanical action by faster rotation of tool causes additional energy input eventually leads to the higher heat generation and increase in welding temperature. Therefore, judicious control over rotational speed is an important step to produce high-quality FSW joints.

3.1(b) Influence of Welding Speed on temperature-time History

Table 6 shows the comparison of experimental and simulation results in terms of welding speed on the thermal behaviour of the joints. On varying the welding speed only and keeping the tool rotational speed constant (1000 RPM), it is found that the peak temperature of sample S3 with 56 mm/min of welding speed is 305.115 °C while the peak temperature of sample S1 with 28 mm/min of welding speed is 319.271 °C. It is noticeable that the welding speed mainly affects the movement of the plasticised material from the front to the rear side of the rotating pin. The fast movement of the tool may cause improper disposal of molten material leading to the welding defect and inferiors the joint performance. As the tool moves faster, the time available to transfer the heat is less and hence lower the temperature is evolved. In this event also, the simulation results (shown in Figure 6) hold a decent correlation with the temperature measured from experimental trials.

Table 6: Effect of welding speed rate on peak temperature, on keeping the tool rotational speed (rpm) constant

Sample	**RPM**	***v***	T_E^{max}	T_S^{max}	**Δ**
S1	1000	28	319.271	328.38	2.85
S3	1000	56	305.115	311.67	2.15

It can be seen from the Figure 7 that the peak temperature of the sample S1 with 28 mm/min of welding speed is much higher than the peak temperature of sample S3 with 56 mm/min of welding speed. The deviation percentages are accounted as less than 5% (see Table 6), which further supports the acceptance of the proposed model.

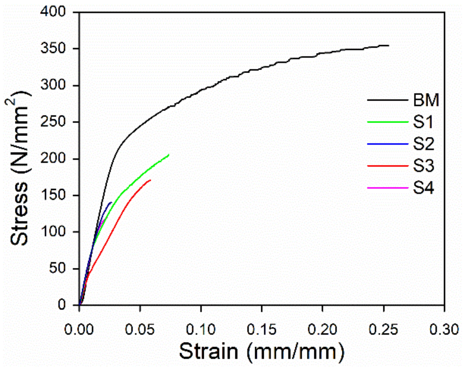

Figure 8: Stress-strain curve of fabricated friction stir welded samples

3.2 TENSILE PROPERTIES

The engineering stress-strain curve of all four welds is shown in Figure 8. It can be noted that the tensile strength recorded for all the specimens found to be well below than that of the unwelded specimen. The joint efficiency and the tensile strength of all the welded samples are summarised in Table 7. It is observed that the joint efficiency found to be a maximum of 60.28% in the case of sample S1 and a minimum value of 35.22% for sample S4. However, in some cases, poor joint efficiency has been recorded (Sample S2 & S3).

Table 7: Joint efficiency and tensile strength of the fabricated friction stir welded samples

S No.	Sample	UTS	Welding Efficiency (%)
01	S1	213.49	60.28
02	S2	146.75	41.43
03	S3	173.38	48.95
04	S4	124.74	35.22
05	Base Metal	354.18	100.00

It is evident from the tensile curves that the tensile strength of the weld joints are not only affected by the tool rotational speed but also the welding speed plays an important role in obtaining the joint performance.

3.2 (a) Influence of Tool Rotational Speed on Tensile Properties

It is observed that with the increase in rotational speed (RPM), the tensile strength increases, and this is true for both the level of welding speed. This is illustrated in figure 9. This can be explained as the high rotational speed produces a large amount of heat which enhance recrystallisation rate and yields better grain refinement leads to the improvement in the strength of the joint.

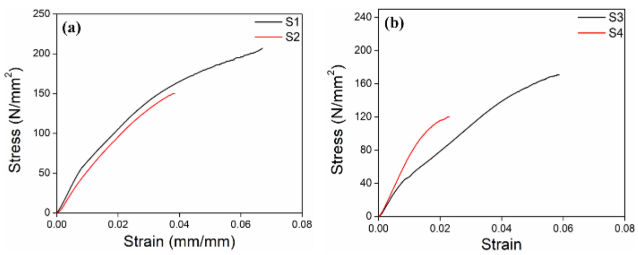

Figure 9: Effect of tool rotational speed in the assessment of engineering stress-strain curve (a) sample S1 & S2 welded with 1000 rpm and 710 rpm respectively at 28 mm/min of welding speed (b) sample S3 & S4 welded with 1000 rpm and 710 rpm respectively at 56 mm/min of welding speed.

3.2 (b) Influence of Welding Speed on Tensile Properties

Figure 10 shows the effect of welding speed on the tensile behaviour of the joints. It is clear from the Figure that samples S1 & S2 with lower welding speed produces joints exhibits higher tensile strengths as compared to the samples S3 & S4 welded with higher welding speed. This can be explained as welding speed is responsible for the movement of the plasticised material from the front to the back of the rotating pin. The faster the tool moves forward; the dumping of molten material becomes improper. The welding speed also influences the heat generated from the tool movement. Thus, it can be said that the faster the tool moves, lower is the temperature evolved. If the forward motion is too slow, then there will be overheating leading to wormholes and grain coarsening which results in lowering of the strength.

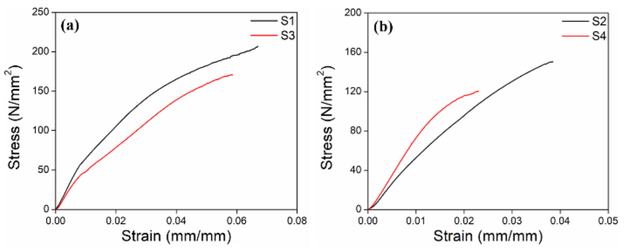

Figure 10: Effect of welding speed on the engineering stress-strain plots (a) sample S1 & S3 welded with tool T1 at 1000 rpm and welding speed of 28 mm/min and 56 mm/min respectively, (b) sample S2 & S4 welded with 710 rpm and welding speed of 28 mm/min and 56 mm/min respectively.

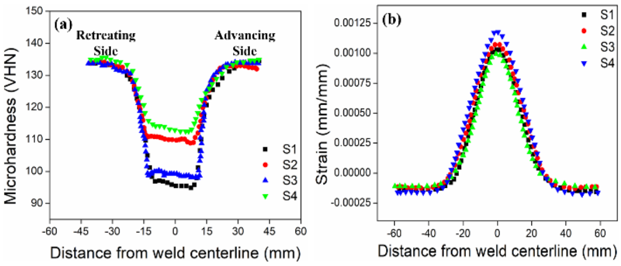

Figure 11: (a) Microhardness variation as a function of transverse distance from weld centreline obtained from experiment; (b) strain variation as a function of transverse distance from weld centreline obtained from the thermo-mechanical model.

3.3 MICROHARDNESS AND STRAIN PROFILE

Figure 11(a) shows the variation of microhardness with transverse distance from weld centreline recorded experimentally. The microhardness profiles indicate the work-hardened state of the parent metal with a hardness value of around 125-135 VHN as against the usual range of the hardness of 95-100 VHN under the annealed condition of AA5083. It can be noticed that lower hardness value lies in the region near the weld centreline.

Not only this, but the region of lower hardness value is also almost limited within 10-15mm on either side of weld centreline. In all the specimens, the hardness values of the nugget zone (NZ) have been recorded in the range of 90-100 VH which is approximately 20-25% lower than the hardness value range of base metal (BM) which is of about 130-135 VH. This result holds a strong agreement with the previously reported work in this alloy (Peel *et al.*, 2006) in terms of the variation, breadth of profile and especially the region of lower hardness value.

It is also evident from Figure 11(a) that both the parameters, i.e., tool rotational speed and welding speed, have a significant impact upon the plateau of the hardness profile. It is clearly observed that with higher welding speed, the hardness value increases. This is because, higher welding speed produces much more finer grains which increase hardness values (Peel *et al.*, 2006)(Peel *et al.*, 2003). Due to the higher welding speed, the time available for heat transfer is less, which restricts the grain growth phenomenon. Thus, grains remain finer, which increases the hardness value. Also, the tool rotational speed is in inverse relation with the hardness values. Higher rotational speed not only causes the refinement of the grains, but the excess energy left after the refinement process promotes the grain growth. Thus, the hardness value falls with an increase in the tool rotational speed. It can also be noted that the profile is somewhat asymmetric. The hardness values measured on the retreating side is around 5-6% higher than that of the measured hardness values on advancing side (from Figure 11(a)). This is so because, retreating side experiences higher thermal gradient which causes a considerable increase in the transverse residual stresses on that side as compared to the residual stresses on the other side.

Figure 11(b) shows the simulated strains generated along with the transverse distance from the weld centreline during the FSW process. Since the highest temperature and the strain occur at the nugget regions and in turn resulted in the attainment of maximum grain refinements in this zone. Therefore, the expected microstructure of this region is refined equiaxed grains with low dislocation density which shows the lower hardness than that of the elongated restrained base metal region. Nevertheless, thus the simulated strain profile well correlates with the hardness profile.

3.4 RESIDUAL STRESSES

Figure 12 shows the variation of the longitudinal and transverse component of residual stresses on either side of the weld centreline. The generated profile is found to be in decent agreement in-general with the previously reported work (Lombard *et al.*, 2009) in terms of the position and breadth of NZ and the region of tensile stresses. Figure 12(a) depicts that the magnitude of maximum longitudinal residual stress is around 60-80% higher than the magnitude of transverse residual stresses presented in Figure 12(b). The positive tensile stresses are within the region of 25mm around the tool axis. This is mainly because of the action of high shear forces on the peripheral region of tool shoulder.

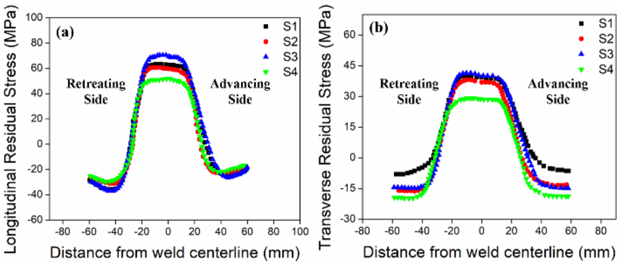

Figure 12: Variation of (a) longitudinal and, (b) transverse residual stress with transverse distance on either side of weld centreline obtained from the thermo-mechanical model.

Also, these tensile stress regions are because of the plunging action of the tool along the axial path of the tool. A similar observation has been reported in (Masubuchi, 1980). The tensile stress within the NZ is not constant and varies within the vicinity of the tool limited to 7-8mm on either side of weld centreline. This variation might be because of the penetration of the tool pin, which induces plastic flow, and this is how the thermo-mechanical phenomena linked with the FSW process is correlated with the residual stresses., These tensile stresses at the vicinity of NZ, are normalised by the compressive stresses generated near the base metal. The positive stresses cause the expansion of the material, and at the same time, this expansion is restricted by the fixtures provided at the end of the weld plates.

3.4 (a) Influence of Welding Speed on Residual Stresses

The longitudinal and transverse FSW residual stress distribution obtained from the simulation results are shown in figure 13, 14, 15 & 16 for different welding conditions. In these figures, the X-X line represents the axis-aligned in the transverse direction to the longitudinal weld centreline.

Figure 13,14 and the profile shown in Figure 12, depict the effect of welding speed on the longitudinal and transverse residual stresses. The welding speed is in direct relation with the residual stress, i.e., higher welding speed induces higher residual stress. Sample S3 with welding speed 56 mm/min is having higher longitudinal stress of 68.9 MPa (shown in Figure 13(b)) as compared to the sample S1 which has lower welding speed of 28 mm/min, resembling a peak longitudinal stress value of 61.3 MPa (shown in Figure 13(a)).

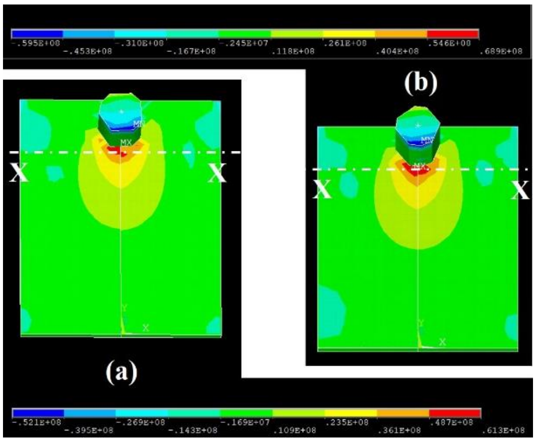

Figure 13: Simulated longitudinal residual stress of (a) sample S1 with 1000 rpm & 28 mm/min and (b) sample S3 with 1000 rpm & 56 mm/min of welding speed.

The similar behaviour has been noted in the case of transverse residual stresses as well. Sample S3 with welding speed 56 mm/min is revealing higher transverse residual stress of 36.5 MPa (shown in Figure 14(b)) in contrast to the sample S1 fabricated at a lower welding speed of 28 mm/min and resembles a peak transverse residual stress value of 38.2 MPa (see Figure 14(a)). This is because of the lower availability of the heat input from faster tool travel which results in inadequate deposition of the plasticised material. Time available to transfer the available heat is low, and this restricts the thermal expansion upon cooling, which led to the lowering of the residual stress of the joint fabricated with the higher welding speed. Similar observations are reported in the previously published work (Peel *et al.*, 2006)(Lombard *et al.*, 2009).

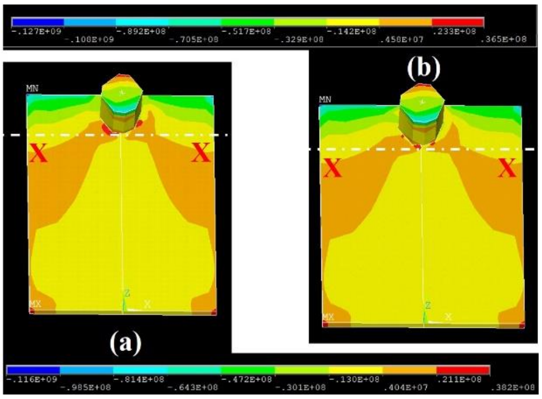

Figure 14: Simulated transverse residual stress of (a) sample S1 with 1000 rpm & 28 mm/min and (b) sample S3 with 1000 rpm & 56 mm/min of welding speed

3.4 (b) Influence of Tool Rotational Speed (RPM) on Residual Stresses

Figure 12, 15 & 16 illustrates the marginal effect of tool rotational speed on the peak residual stresses. The tool rotational speed nominal impact on the residua; stress, i.e., increased rotational speed resulted in marginal increase residual stress. Sample S2 with a rotational speed of 710 RPM is having lower longitudinal stress of 60.1 MPa (shown in Figure 15(b)) as compared to the sample S1 which has a higher rotational speed of 1000 RPM, resembling a peak longitudinal stress value of 61.3 MPa (shown in Figure 15(a)).

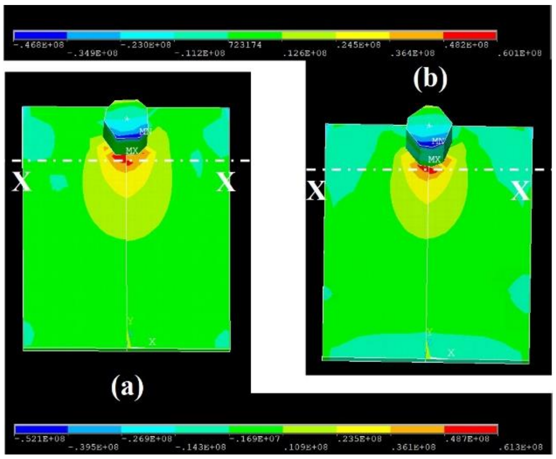

Figure 15: Simulated longitudinal residual stress of (a) sample S1 with 1000 rpm & (b) sample S2 with 710 rpm and 28 mm/min of welding speed

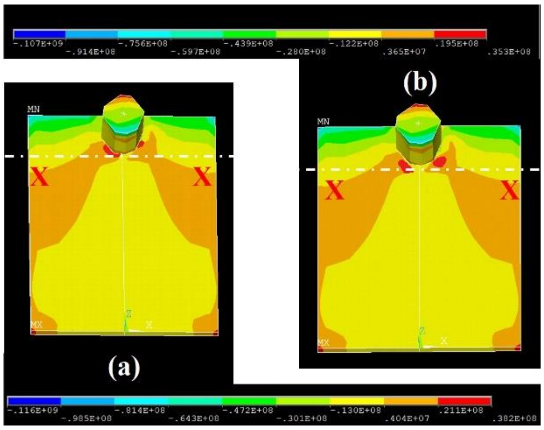

Figure 16: Simulated transverse residual stress of (a) sample S1 with 1000 rpm & (b) sample S2 with 710 rpm and 28 mm/min of welding speed

The effect of tool rotational speed is not only limited to longitudinal residual stress, but transverse residual stress also follows the same behaviour. Sample S2 with lower rotational speed 710 RPM has lower transverse residual stress of 35.3 MPa (shown in Figure 16(b)) as compared to the sample S1 which has elevated rotational speed of 1000 RPM resembles a peak transverse residual stress value of 38.2 MPa (shown in Figure 16(a)). This observation is supported by the statement that, larger availability of the heat input from faster tool rotation. The time available for heat propagation is sufficient to cause thermal expansion. This thermal expansion strengthens the temperature gradient, which is the main cause of increases residual stress with the rise in tool rotational speed.

3.4 (c) Process Property Correlation

The residual stresses in FSW joints are caused by a combined thermo-mechanical effect resulted from the thermal shocks and the plasticised materials flow under the severe deformation of the material. The induce residual stresses have both tensile and compressive zones along and across the weld centreline. The spread of the longitudinal residual stress developed a tensile zone originated from the centre of the tool and includes weld-nugget zone, HAZ and TMAZ. Parent metal generally falls upon the compressive zones. This is schematically illustrated in Figure 17. Also, transverse residual stresses are developed with a significantly low magnitude as compared to the longitudinal residual stresses.

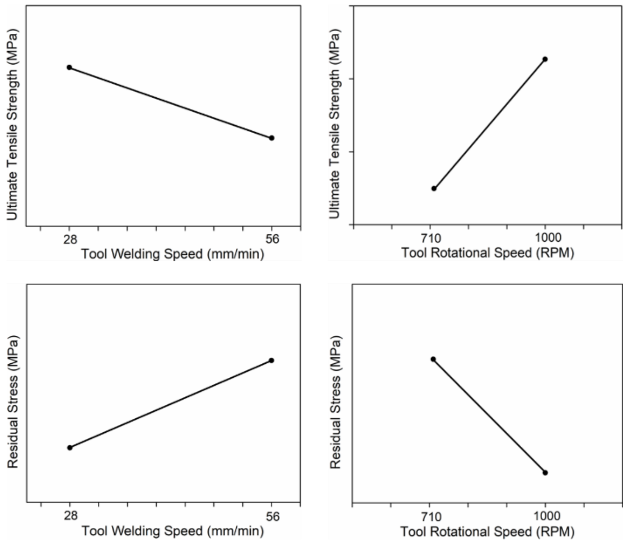

Figure 17 Correlation between process parameters (tool rotational speed and welding speed) and material properties (ultimate tensile strength and residual stress).

The corelation study between the FSW operational parameters such as welding speed (mm/min) and the tool rotational (rpm) with the longitudinal residual stresses and the tensile strength of the joint revealed a worthy relationship. With an increase of welding speed from 28 mm/min to 56 mm/min the longitudinal residual stress increases from 61.3MPa to 68.3MPa presenting a direct relation and the tensile strength decreases 213.49MPa to 173.38MPa, indicating an inverse relation. Nevertheless, the tool rotational speed shows inverse relation with the residual stresses and direct with tensile strength. The measure of residual strength in FSW joint is important in the assessment of fatigue strength and the ductility. Although, correlating the residual stresses with tensile strength in isolation is an inconclusive analysis; however, this study indicates that the existence of high residual stresses diminished the mechanical strength of the joints and vice versa.

4. CONCLUSION

The present study successfully implemented the FEM technique to develop the thermomechanical model of the FSW process for AA5083 material and used to demonstrate the process-structure-property correlation study of FSW joints. The FE simulation outcomes attained from the proposed thermo-mechanical model holds a strong correlation with the peak temperature acquired from the experimental trials. The deviation percentages are accounted within 5% and which validates the FE model and accord to use for further analysis of process-structure-property correlation study of the FSW process reported in this article. The simulation results of thermal history, mechanical strain distribution and residual stress obtained from the proposed thermo-mechanical model demonstrated the experimentally recorded thermal history, EBSD microstructural observation and mechanical properties. The study effectively bridges the process property correlation and establishes the role of the FSW process parameter such as rotational speed and welding speed for this alloy.

5. REFERENCES

1. AYER, R. *et al.* (2005) 'Interface structure in a Fe-Ni friction stir welded joint', *Scripta Materialia*, 53(12), pp. 1383–1387. doi: 10.1016/j.scriptamat.2005.08.042.
2. BJØRNEKLETT, B. I. *et al.* (1999) 'A process model for the heat-affected zone microstructure evolution in Al-Zn-Mg weldments', *Metallurgical and Materials Transactions A: Physical Metallurgy and Materials Science*, 30(10), pp. 2667–2677. doi: 10.1007/s11661-999-0307-2.
3. BUFFA, G. *et al.* (2006a) 'A continuum based fem model for friction stir welding - Model development', *Materials Science and Engineering A*, 419(1–2), pp. 389–396. doi: 10.1016/j.msea.2005.09.040.
4. BUFFA, G. *et al.* (2006b) 'Design of the friction stir welding tool using the continuum based FEM model', *Materials Science and Engineering A*, 419(1–2), pp. 381–388. doi: 10.1016/j.msea.2005.09.041.
5. ÇAM, G. and MISTIKOGLU, S. (2014) 'Recent developments in friction stir welding of al-Alloys', *Journal of Materials Engineering and Performance*, 23(6), pp. 1936–1953. doi: 10.1007/s11665-014-0968-x.
6. CHAO, Y. J., QI, X. and TANG, W. (2003) 'Heat Transfer in Friction Stir Welding—Experimental and Numerical Studies', *Journal of Manufacturing Science and Engineering*, 125(1), p. 138. doi: 10.1115/1.1537741.
7. CHEN, C. M. and KOVACEVIC, R. (2003) 'Finite element modeling of friction stir welding - Thermal and thermomechanical analysis', *International Journal of Machine Tools and Manufacture*, 43(13), pp. 1319–1326. doi: 10.1016/S0890-6955(03)00158-5.
8. COLEGROVE, P. A. *et al.* (2013) 'Model for predicting heat generation and temperature in friction stir welding from the material properties Model for predicting heat generation and temperature in friction stir welding from the material properties', 1718. doi: 10.1179/174329307X197539.
9. DICKERSON, T., SHI, Q. and SHERCLIFF, H. R. (2003) 'Heat flow into friction stir welding tools', *4th international symposium on friction stir welding, USA*, (May), pp. 1–11. doi: 10.1093/ejo/cjr127.
10. DONG, P. *et al.* (2013) 'Coupled thermomechanical analysis of friction stir welding process using simplified models', *Science and Technology of Welding and Joining*, 6(5), pp. 281–287. doi: 10.1179/136217101101538884.
11. FRIGAARD, Ø., GRONG, Ø. and MIDLING, O. T. (2001) 'A process model for friction stir welding of age hardening aluminum alloys', *Metallurgical and Materials Transactions A*, 32(5), pp. 1189–1200. doi: 10.1007/s11661-001-0128-4.
12. JATA, K. V. (2009) 'Friction Stir Welding of High Strength Aluminum Alloys', *Materials Science Forum*, pp. 1701–1712. doi: 10.4028/www.scientific.net/msf.331-337.1701.
13. JIN, H. *et al.* (2001) 'Characterisation of microstructure and texture in friction stir welded joints of 5754 and 5182 aluminium alloy sheets', *Materials Science and Technology*. Taylor & Francis, 17(12), pp. 1605–1614. doi: 10.1179/026708301101509674.
14. KOUADRI-HENNI, A. and BARRALLIER, L. (2014) 'Mechanical properties, microstructure and crystallographic texture of magnesium AZ91-D alloy welded by friction stir welding (FSW)', *Metallurgical and Materials Transactions A: Physical Metallurgy and Materials Science*, 45(11), pp. 4983–4996. doi: 10.1007/s11661-014-2381-3.
15. KUMAR THIMMARAJU, P., ARKANTI, K. and CHANDRA MOHAN REDDY, G. (2018) 'Parametric Analysis of Friction Stir Welding Process', *Materials Today: Proceedings*, 5(13), pp. 26981–26989. doi: 10.1016/j.matpr.2018.09.001.
16. LOMBARD, H. *et al.* (2009) 'Effect of process parameters on the residual stresses in AA5083-H321 friction stir welds', *Materials Science and Engineering A*, 501(1–2), pp. 119–124. doi: 10.1016/j.msea.2008.09.078.
17. MASUBUCHI, K. (1980) 'Analysis of Welded Structures Pergammon Press'. Oxford.
18. MISHRA, R. S. and MA, Z. Y. (2005) 'Friction stir welding and processing', *Materials Science and Engineering R: Reports*, 50(1–2), pp. 1–78. doi: 10.1016/j.mser.2005.07.001.
19. MOHAN, R. *et al.* (2014) 'Finite element modeling for maximum temperature in friction stir welding of AA1100 and optimisation of process parameter by taguchi method', *International Journal of research in engineering and technology*, 3(5), pp. 728–733.
20. PEEL, M. *et al.* (2003) 'Microstructure, mechanical properties and residual stresses as a function of welding speed in aluminium AA5083 friction stir welds', *Acta Materialia*, 51(16), pp. 4791–4801. doi: 10.1016/S1359-6454(03)00319-7.
21. PEEL, M. J. *et al.* (2006) 'Dissimilar friction stir welds in AA5083-AA6082. Part I: Process

parameter effects on thermal history and weld properties', *Metallurgical and Materials Transactions A: Physical Metallurgy and Materials Science*, 37(7), pp. 2183–2193. doi: 10.1007/BF02586138.

22. PRASANNA, P., RAO, B. S. and RAO, G. K. M. (2010) 'Finite element modeling for maximum temperature in friction stir welding and its validation', *The International Journal of Advanced Manufacturing Technology*, 51(9–12), pp. 925–933. doi: 10.1007/s00170-010-2693-4.
23. REYNOLDS, A. P., HOOD, E. and TANG, W. (2005) 'Texture in friction stir welds of Timetal 21S', *Scripta Materialia*, 52(6), pp. 491–494. doi: 10.1016/j.scriptamat.2004.11.009.
24. SCHMIDT, H., HATTEL, J. and WERT, J. (2004) 'An analytical model for the heat generation in friction stir welding', *Modelling and Simulation in Materials Science and Engineering*, 12(1), pp. 143–157. doi: 10.1088/0965-0393/12/1/013.
25. SOUNDARARAJAN, V., ZEKOVIC, S. and KOVACEVIC, R. (2005) 'Thermo-mechanical model with adaptive boundary conditions for friction stir welding of Al 6061', *International Journal of Machine Tools and Manufacture*, 45(14), pp. 1577–1587. doi: 10.1016/j.ijmachtools.2005.02.008.
26. THOMAS, W. M. *et al.* (1991) *Friction stir butt welding. Application No.* PCT/ GB92/02203 and *GB Patent Application No.* 9125978.8 and *US Patent Application No.* 5,460,317.
27. UYYURU, R. K. and KAILAS, S. V. (2006) 'Numerical Analysis of Friction Stir Welding Process', *Journal of Materials Engineering and Performance*, 15(5), pp. 505–518. doi: 10.1361/105994906X136070.
28. ZHU, X. K. and CHAO, Y. J. (2002) 'Effects of temperature-dependent material properties on welding simulation', *Computers and Structures*, 80(11), pp. 967–976. doi: 10.1016/S0045-7949(02)00040-8.
29. ZHU, X. K. and CHAO, Y. J. (2004a) 'Numerical simulation of transient temperature and residual stresses in friction stir welding of 304L stainless steel', *Journal of Materials Processing Technology*, 146(2), pp. 263–272. doi: 10.1016/j.jmatprotec.2003.10.025.
30. ZHU, X. K. and CHAO, Y. J. (2004b) 'Numerical simulation of transient temperature and residual stresses in friction stir welding of 304L stainless steel', *Journal of Materials Processing Technology*, 146(2), pp. 263–272. doi: 10.1016/j.jmatprotec.2003.10.025.